Measurement of Autler-Townes and Mollow transitions in a strongly driven superconducting qubit

M. Baur,[1] S. Filipp,[1] R. Bianchetti,[1] J.M. Fink,[1] M. Göppl,[1] L. Steffen,[1] P.J. Leek,[1] A. Blais,[2] and A. Wallraff[1]

[1]*Department of Physics, ETH Zurich, CH-8093 Zurich, Switzerland*
[2]*Département de Physique, Université de Sherbrooke, Sherbrooke, Québec J1K2R1, Canada*

(Dated: December 24, 2008)

We present spectroscopic measurements of the Autler-Townes doublet and the sidebands of the Mollow triplet in a driven superconducting qubit. The ground to first excited state transition of the qubit is strongly pumped while the resulting dressed qubit spectrum is probed with a weak tone. The corresponding transitions are detected using dispersive read-out of the qubit coupled off-resonantly to a microwave transmission line resonator. The observed frequencies of the Autler-Townes and Mollow spectral lines are in good agreement with a dispersive Jaynes-Cummings model taking into account higher excited qubit states and dispersive level shifts due to off-resonant drives.

When a two-level system is driven on resonance with a strong monochromatic field, the excited state population undergoes coherent Rabi oscillations. This coherent process is reflected in the appearance of two sidebands offset by the Rabi frequency from the main qubit transition in the spectrum. This leads to a three peaked fluorescence spectrum referred to as the Mollow triplet [1]. When probing transitions into a third atomic level, two characteristic spectroscopic lines separated by the Rabi frequency appear, a feature which is called the Autler-Townes doublet [2]. The Mollow triplet and the Autler-Townes doublet were observed for the first time in an atomic beam of sodium [3] and in a He-Ne discharge laser [4], respectively. Later they have been measured in single molecules [5, 6], single atoms [7] and more recently also in quantum dots [8–10].

Here we present experiments in which we spectroscopically probe Mollow sideband and Autler-Townes transitions in a strongly driven superconducting quantum electronic circuit with discrete energy levels [11]. The properties of superconducting qubits dressed by strong drive fields have also been studied experimentally in Refs. 12, 13. Other examples of spectroscopic techniques used in the context of superconducting qubits include multi-photon spectroscopy with photons of the same [14, 15] and of different frequencies [16], amplitude spectroscopy [17], side-band spectroscopy of coupled systems [18] and pump/probe spectroscopy [19]. In several experiments it has also been shown that artifical atoms based on superconducting circuits show quantum optical effects as real atoms do [20]. Single photons [21], Fock states generation [22] and lasing effects in a Cooper pair box [23] have been demonstrated.

In the experiments presented here, we use a version of the Cooper pair box [24], called transmon qubit [25], as our multilevel quantum system. States of increasing energies are labelled $|l\rangle$ with $l = g, e, f, h, i, \ldots$ The transition frequency ω_{ge} between the ground $|g\rangle$ and first excited state $|e\rangle$ is approximated by $\hbar\omega_{ge} \approx \sqrt{8E_C E_J^{\max}|\cos 2\pi\Phi/\Phi_0|} - E_C$ [25], where $E_C/h = 233\,\mathrm{MHz}$ is the charging energy and $E_J^{\max}/h = 32.8\,\mathrm{GHz}$ is the maximum Josephson energy. The transition frequency ω_{ge} can be controlled by an external magnetic flux Φ applied to the SQUID loop formed by the two Josephson junctions of the qubit. The transition frequency from the first $|e\rangle$ to the second excited state $|f\rangle$ is given by $\omega_{ef} = \omega_{ge} - \alpha$, where $\alpha \approx 2\pi E_C/h$ is the qubit anharmonicity [25]. The qubit is strongly coupled to a coplanar waveguide resonator with resonance frequency $\omega_r/2\pi = 6.439\,\mathrm{GHz}$ and photon decay rate $\kappa/2\pi \approx 1.6$ MHz. A schematic circuit diagram of the setup is shown in Fig 1(a).

When the ground to first excited state transition of the qubit is in resonance with the resonator ($\Delta_{ge} = \omega_{ge} - \omega_r = 0$), the strong coupling gives rise to the vacuum Rabi mode splitting [15, 19, 26] from which we have determined a dipole coupling strength $g_{ge}/2\pi = 133\,\mathrm{MHz}$ between the first two energy levels. In the non-resonant regime, where the qubit is far detuned from the resonator ($|\Delta_{ge}| \gg g_{ge}$), the system is described by the generalized Jaynes-Cummings Hamiltonian in the dispersive limit [25]

$$H_{JC} \approx \hbar\Big[\omega_r - \chi_{ge}|g\rangle\langle g| + \sum_{l=e,f,\ldots}(\chi_{l-1,l} - \chi_{l,l+1})|l\rangle\langle l|\Big]a^\dagger a + \hbar\omega_g|g\rangle\langle g| + \hbar\sum_{l=e,f,\ldots}(\omega_l + \chi_{l-1,l})|l\rangle\langle l|. \quad (1)$$

In the first term, χ_{ge} and $(\chi_{l-1,l} - \chi_{l,l+1})$ describe both the qubit-state dependent resonator frequency shift and the ac-Stark shift of the qubit energy levels [25, 27, 28]. The dispersive frequency shift $\chi_{l,l+1} = g_{l,l+1}^2/\Delta_{l,l+1}$ is determined by the coupling strength $g_{l,l+1}$ between the levels $|l\rangle$ and $|l+1\rangle$ mediated by the resonator field and the detuning frequency $\Delta_{l,l+1} = \omega_{l,l+1} - \omega_r$. a ($a^\dagger$) are the annihilation (creation) operators of the single mode field. In the last term, $\chi_{l-1,l}$ describes the Lamb shift of the transmon levels due to the dispersive coupling of the qubit to vacuum fluctuations in the resonator [29].

We measure the Autler-Townes and the Mollow spectral lines according to the scheme shown in Fig. 1(b).

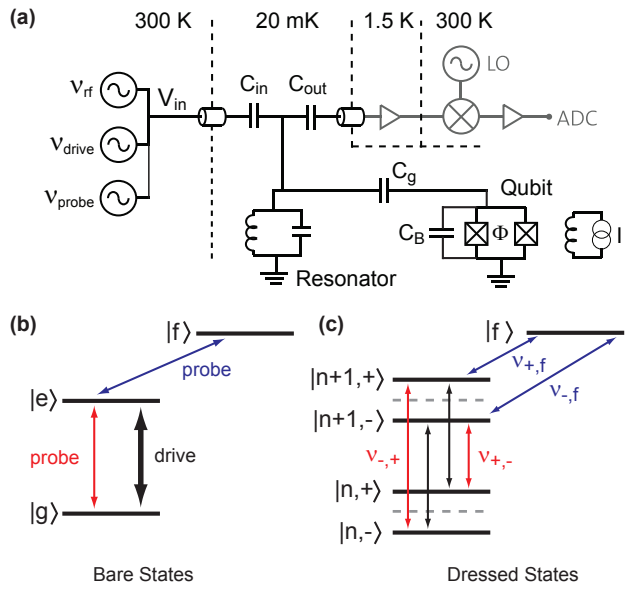

FIG. 1: (a) Simplified circuit diagram of the measurement setup analogous to the one used in Ref. [19]. In the center at the 20 mK stage, the qubit is coupled capacitively through C_g to the resonator, represented by a parallel LC oscillator, and the resonator is coupled to the input and output transmission lines over capacitances $C_{\rm in}$ and $C_{\rm out}$. Three microwave signal generators are used to apply the measurement $\nu_{\rm rf}$ and drive and probe tones $\nu_{\rm drive/probe}$ to the input port of the resonator. The transmitted measurement signal is then amplified by an ultra-low noise amplifier at 1.5 K, down-converted with an IQ-mixer and a local oscillator (LO) to an intermediate frequency at 300K and digitized with an analog-to-digital converter (ADC). (b) Energy-level diagram of a bare three-level system with states $|g\rangle, |e\rangle, |f\rangle$ ordered with increasing energy. Drive and probe transitions are indicated by black and red/blue arrows, respectively. (c) Energy-level diagram of the dipole coupled dressed states with the coherent drive tone. Possible transitions induced by the probe tone between the dressed states and the third qubit level ($\nu_{-,f}$,$\nu_{+,f}$) and between the dressed states ($\nu_{-,+}, \nu_{+,-}$) are indicated with blue and red arrows.

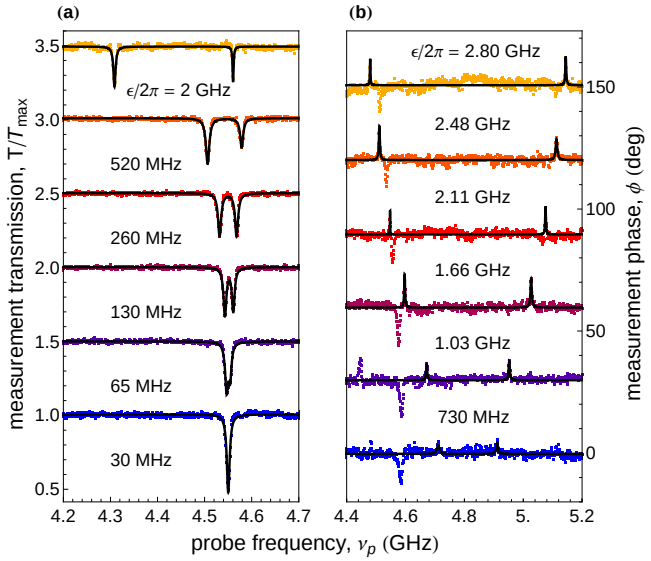

FIG. 2: (a) Autler-Townes spectrum as a function of drive amplitude ε. Traces are normalized to the maximum transmission through the resonator, and separated from each other with a vertical offset of 0.5. (b) Mollow spectrum in phase. Traces are offset by 30 degrees. Black solid lines are fits to Lorentzians. Peaks not fitted with Lorentzians correspond to the phase response of the Autler-Townes doublet.

First, we tune the qubit to the frequency $\omega_{ge}/2\pi \approx 4.811\,$GHz, where it is strongly detuned from the resonator by $\Delta/2\pi = 1.63\,$GHz. We then strongly drive the transition $|g\rangle \rightarrow |e\rangle$ with a first microwave tone of amplitude ε applied to the qubit at the fixed frequency $\omega_d = 4.812\,$GHz. The drive field is described by the Hamiltonian $H_d = \hbar\varepsilon(a^\dagger e^{-i\omega_d t} + a e^{i\omega_d t})$ where the drive amplitude ε is given in units of a frequency. The qubit spectrum is then probed by sweeping a weak second microwave signal over a wide range of frequencies ω_p including ω_{ge} and ω_{ef}. Simultaneously, amplitude T and phase ϕ of a microwave signal applied to the resonator are measured [26]. We have adjusted the measurement frequency to the qubit state-dependent resonance of the resonator under qubit driving for every value of ε. Figures 2(a) and (b) show the measurement response T and ϕ for selected values of ε. For drive amplitudes $\varepsilon/2\pi > 65\,$MHz, two peaks emerge in amplitude from the single Lorentzian line at frequency ω_{ef} corresponding to the Autler-Townes doublet, see Fig. 2(a). The signal corresponding to the sidebands of the Mollow triplet is visible at high drive amplitudes $\varepsilon/2\pi > 730\,$MHz in phase, see Fig. 2(b). Black lines in Fig. 2 are fits of the data to Lorentzians from which the dressed qubit resonance frequencies are extracted.

An intuitive model explaining those two effects can be given in the dressed state picture [30]. In the situation where the drive is exactly on resonance with the qubit, the bare states $|n, g\rangle$ and $|n-1, e\rangle$ of the uncoupled atom-field system are degenerate, where n is the average number of photons in the coherent drive. The dipole coupling splits the energy levels by the Rabi frequency $\hbar\Omega_R$ and forms an energy ladder of doublets separated by the energy of the drive photons $\hbar\omega_d$. The new dressed eigenstates dipole coupled to the field are symmetric and antisymmetric superpositions of the bare states $|n, \pm\rangle = |n, g\rangle \pm |n-1, e\rangle$, see Fig. 1(c). In the limit $n \gg \sqrt{n}$, the allowed transitions between dressed state doublets appear at frequencies $\omega_0 = \omega_{ge}$, $\omega_{+,-} = \omega_{ge} - \Omega_R$ and $\omega_{-,+} = \omega_{ge} + \Omega_R$ which are the central line and the two sidebands of the Mollow triplet, respectively, indicated by black and red arrows in Fig. 1c. The central line is not observed in our measurements as the corresponding transition is completely saturated by the strong drive tone. Similarly, transitions from one

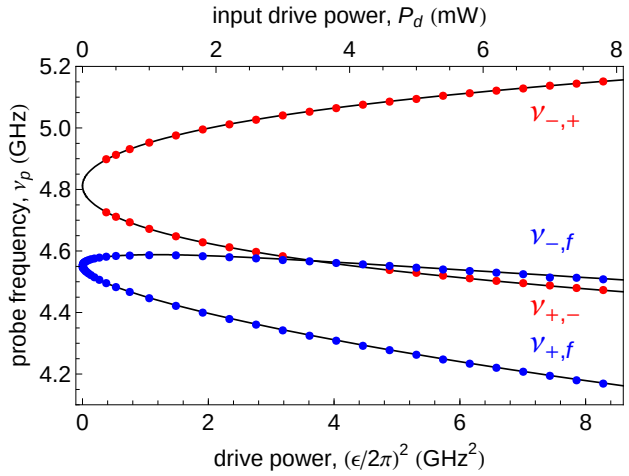

FIG. 3: Measured Autler-Townes doublet (blue dots) and Mollow triplet sideband frequencies (red dots) *vs.* drive power P_d at a fixed drive frequency $\omega_d/2\pi = 4.812\,\mathrm{GHz}$. Black solid lines are transition frequencies calculated by numerically diagonalizing the Hamiltonian (3) taking into account the lowest 5 transmon levels.

pair of dressed levels $|n+1,\pm\rangle$ to the third level $|f\rangle$ at frequencies $\omega_{\pm,f} = \omega_{ef} \mp \Omega_R/2$ correspond to the Autler-Townes doublet. The splitting of the dressed states is only well resolved, when Ω_R is considerably larger than the qubit linewidth.

The frequencies of the Autler-Townes doublet (blue data points) and of the Mollow triplet sidebands (red data points) extracted from the Lorentzian fits in Fig. 2(a) and (b) are plotted in Fig. 3. The splitting of the spectral lines in pairs separated by Ω_R and $2\Omega_R$, respectively, is observed for Rabi frequencies up to $\Omega_R/2\pi \approx 300\,\mathrm{MHz}$ corresponding to about 6% of the qubit transition frequency ω_{ge}.

In the simplest model, the continuous classical drive at frequency ω_d is expected to induce Rabi oscillations between the qubit levels $|l\rangle$ and $|l+1\rangle$ at the frequency [31]

$$\Omega_{l,l+1} \approx \frac{2\varepsilon g_{l,l+1}}{\omega_r - \omega_d}, \qquad (2)$$

depending linearly on the drive amplitude ε. Therefore, one would expect that the strong drive at the qubit transition frequency $\omega_d \approx \omega_{ge}$ should lead to a square-root dependence of the Autler-Townes and Mollow spectral lines on the drive power $P_d \propto \varepsilon^2$. However, the Autler-Townes spectral lines show a clear power dependent shift, see Fig. 3, and the splitting of both pairs of lines scales weaker than linearly with ε.

These effects can be fully understood calculating the different transition frequencies by numerically diagonalizing the Jaynes-Cummings Hamiltonian in the dispersive limit including the coherent drive on the qubit

$$H \approx H_{JC} + \sum_l \frac{\Omega_{l,l+1}}{2}(|l\rangle\langle l+1|e^{i\omega_d t} + h.c.). \qquad (3)$$

Here we take into account only the drive terms between nearest neighbor energy levels since other transitions are strongly suppressed due to the near harmonicity of the transmon [25]. This model is in good agreement with our data when considering the lowest 5 qubit levels, see solid black lines in Fig. 3. Because of the low anharmonicity [25] and large drive amplitude, many qubit levels must be included in the description. The calibration factor between the externally applied drive amplitude and ε is the only free parameter in the fit.

Numerical diagonalization of Eq. (3) also leads to a qualitative understanding of the amplitude and phase information contained in the measurement signal. This is done by first calculating the pulled cavity frequencies using the pre-factor of $a^\dagger a$ in H_{JC}. Since the measurement rate is small [32], the measured signal is given by the averaged response of all the dressed-state pulled frequencies contained in the steady-state reached by the qubit under the strong drive tone. In the Autler-Townes configuration, the weak probe tone transfers a small population from the dressed ground and excited states to the dressed f state, resulting in a change in the cavity frequency and a drop of transmitted signal. On the other hand, in the Mollow configuration, population is exchanged by the probe tone from the g to the e dressed-states. At low drive power, the dressed g and e states are equal superpositions of the bare g and e states such that no signal is measured. As the power is increased, these states get dressed in different proportion with f and a signal is measured.

Finally, plotting the difference between the two Autler-Townes spectral lines (blue data points) and the sidebands of the Mollow spectrum (red data points) versus drive amplitude ε, the nonlinearity of the dressed state splitting becomes more apparent, see Fig. 4(a). The dashed line shows the linear dependence of the Rabi frequency Eq. (2) on the drive amplitude ε, which only fits to the data at low ε. The non-linear dependence at high ε, instead, agrees very well only with our full model, black solid line.

To confirm the direct relationship between the measured dressed state splitting frequency and the Rabi oscillation frequency of the excited state population we have also performed time resolved measurements of the Rabi frequency up to 100 MHz, see Fig. 4(c). The extracted Rabi frequencies (orange data points) are in good agreement with the spectroscopically measured Rabi frequencies (blue squares) over the range of accessible ε, as shown in Fig. 4(b)

In conclusion, we have observed the dressed state splitting of the strongly driven energy levels of a superconducting qubit. The frequencies of the Autler-Townes

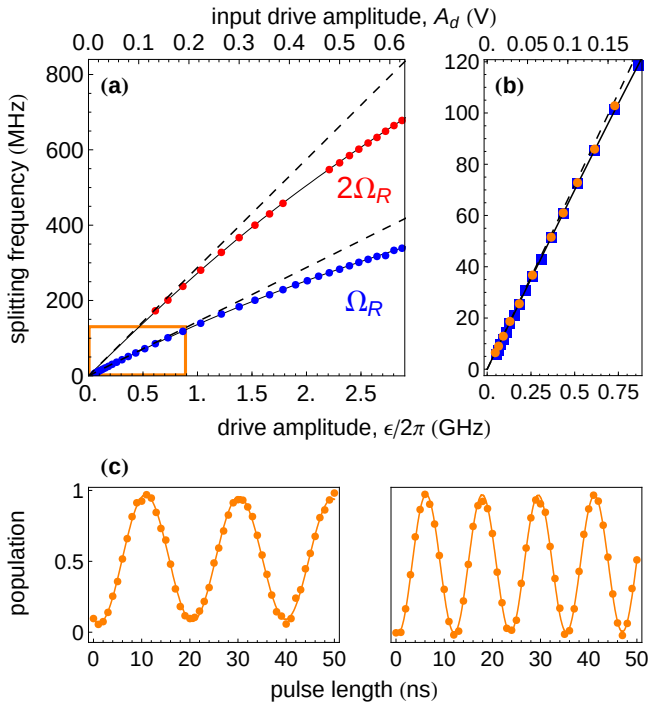

FIG. 4: (a) Extracted splitting frequencies of the Mollow triplet sidebands (red dots) and the Autler-Townes doublet (blue dots) as a function of the drive field amplitude. Dashed lines: Rabi frequencies obtained with Eq. (2). Black solid lines: Rabi frequencies calculated by numerically diagonalizing the Hamiltonian Eq. (3) taking into account 5 transmon levels. (b) Zoom in of the region in the orange rectangle in (a). Orange dots: Rabi frequency Ω_{ge} *vs.* drive amplitude ε extracted from time resolved Rabi oscillation experiments, lines as in (a). (c) Rabi oscillation measurements between states $|g\rangle$ and $|e\rangle$ with $\Omega_R/2\pi = 50\,\mathrm{MHz}$ and $85\,\mathrm{MHz}$.

doublet and sidebands of the Mollow triplet determined using a dispersive measurement technique are in excellent agreement with theory. Splittings corresponding to Rabi frequencies of up to 300 MHz have been observed spectroscopically and are consistent with time resolved measurements. Dressed state splittings have also been suggested to realize tunable coupling between two qubits biased at their optimal points [33]. Our measurements are the first step towards the realization of this protocol.

We thank Maxime Boissonneault and Jay Gambetta for useful discussions. This work was supported by the Swiss National Science Foundation and by ETH Zürich. P.J.L. acknowledges support from the EC via an Intra-European Marie-Curie Fellowship. A.B. was supported by NSERC, CIFAR, FQRNT and Alfred P. Sloan Foundation.

[1] B. R. Mollow, *Phys. Rev.* **188**, 1969 (1969).
[2] S. H. Autler and C. H. Townes, *Phys. Rev.* **100**, 703 (1955).
[3] F. Y. Wu, R. E. Grove, and S. Ezekiel *Phys. Rev. Lett.* **35**, 1426 (1975).
[4] A. Schabert, R. Keil, and P. E. Toschek *Appl. Phys.* **6**, 181 (1975).
[5] G. Wrigge *et al.*, *Nat. Phys.* **4**, 60 (2008).
[6] P. Tamarat *et al.*, *Phys. Rev. Lett.* **75**, 15141517 (1995).
[7] B. Walker *et al.*, *Phys. Rev. Lett.* **75**, 633636 (1995).
[8] X. D. Xu *et al.*, *Science* **317**, 929 (2007).
[9] A. N. Vamivakas *et al.*, arXiv:0806.3707 [cond-mat.mes-hall] (2008).
[10] A. Mullter *et al.*, *Phys. Rev. Lett.* **99**, 187402 (2007).
[11] J. Clarke and F. K. Wilhelm, *Nature* **453**, 1031 (2008).
[12] C. M. Wilson *et al.*, *Phys. Rev. Lett.* **98**, 257003 (2007).
[13] W. D. Oliver *et al.*, *Science* **310**, 1653 (2005).
[14] A. Wallraff *et al.*, *Phys. Rev. Lett.* **90**, 037003 (2003).
[15] L. S. Bishop *et al.*, arXiv:0807.2882v1 [cond-mat.mes-hall]
[16] S. Saito *et al.*, *Phys. Rev. Lett.* **96**, 107001 (2006).
[17] D. M. Berns *et al.*, *Nature* **455**, 51 (2008).
[18] A. Wallraff *et al.*, *Phys. Rev. Lett.* **99**, 050501 (2007).
[19] J. M. Fink *et al.*, *Nature* **454**, 315 (2008).
[20] R. J. Schoelkopf and S. M. Girvin *et al.*, *Nature* **451**, 664 (2008).
[21] A. A. Houck *et al.*, *Nature* **449**, 328 (2003).
[22] M. Hofheinz *et al.*, *Nature* **454**, 310 (2008).
[23] O. Astafiev *et al.*, *Nature* **449**, 588 (2007).
[24] V. Bouchiat *et al.*, *Phys. Scr.* **T76**, 165 (1998).
[25] J. Koch *et al.*, *Phys. Rev. A* **76**, 042319 (2007).
[26] A. Wallraff *et al.*, *Nature* **431**, 162 (2007).
[27] D. I. Schuster *et al.*, *Phys. Rev. Lett.* **94**, 123602 (2005).
[28] D. I. Schuster *et al.*, *Nature* **445**, 515 (2007).
[29] A. Fragner *et al.*, *Science* **322**, 1357 (2008).
[30] C. Cohen-Tannoudji, J. Dupont-Roc, and G. Grynberg, *Atom-Photon Interactions: Basic Processes and Applications* (Wiley Science Paperback Series, 1998).
[31] A. Blais *et al.*, *Phys. Rev. A* **75**, 032329 (2007).
[32] J. Gambetta, *Phys. Rev. A* **77**, 012112 (2008).
[33] C. Rigetti, A. Blais, and M. Devoret, *Phys. Rev. Lett.* **94**, 240502 (2005).